Hindawi Publishing Corporation
Mathematical Problems in Engineering
Volume 2014, Article ID 204165, 9 pages
http://dx.doi.org/10.1155/2014/204165

Research Article

Thermomechanical Modeling of Shape Memory Alloys with Rate Dependency on the Pseudoelastic Behavior

Jin-Ho Roh

School of Aerospace and Mechanical Engineering, Korea Aerospace University, 200-1 Hwajeon, Goyang, Gyeonggi-do 412 791, Republic of Korea

Correspondence should be addressed to Jin-Ho Roh; jinhoroh@kau.ac.kr

Received 21 October 2013; Revised 8 February 2014; Accepted 26 February 2014; Published 29 April 2014

Academic Editor: Mahmoud Kadkhodaei

The loading-rate dependency on the pseudoelastic behaviors of shape memory alloy (SMA) wires is experimentally and numerically investigated. The results are analyzed to estimate the parameters for a thermomechanical constitutive model of SMA wire with strain-rate dependency of the hysteresis behavior. An analytical model of SMAs is developed by using nonconstant parameters during various strain rates. Numerical simulations are performed to demonstrate the accuracy of the improved model.

1. Introduction

Shape memory alloys (SMAs) offer a combination of novel properties such as the shape memory effect and pseudoelasticity. In particular, pseudoelastic behaviors of SMAs are very attractive as damping materials due to their ability to sustain large amounts of strain energy density and to dissipate high levels of work as compared to normal metals. Even though it is interesting to explore SMAs in passive vibration isolation from the host structure, they may also lead to very complex pseudoelastic responses. For example, the rate of temperature variation and the strain rate affect the deformation properties of SMAs, and those properties serve as a basis for the evaluation of SMA thermomechanical behaviors. Therefore, it is very important to establish an appropriate constitutive SMA model for practical applications.

The relationship between the instantaneous SMA temperature and strain rate was first examined experimentally by Mukherjee et al. [1]. Prior experimental data indicated that a strong rate dependence of superelastic NiTi wire existed in the typical frequency range [2]. Nemat-Nasser and Guo [3] studied the dynamic response of NiTi SMAs focusing on their superelastic behavior at various loading rates. Soul et al. [4] investigated the damping properties associated with pseudoelastic SMA behavior in various strain-rate ranges and showed that damping capacity had maximum values at a specific frequency associated with the temperature effect. So, when designing SMA based damping devices for various applications, a constitutive model to accurately predict the stress-strain relationship in the loading-rate range is important. An improved thermomechanical constitutive SMA model was proposed by simply modifying existing models to include the effects of loading frequency [5–8]. Tobushi et al. [2] observed that the critical stresses of phase transformation as well as the slope of the transformation line were affected by strain rates. However, the constitutive models using simple transformation equations or constant parameters for SMAs have limitations in describing the peculiar behavior of SMAs. Ren et al. [9] proposed an improved Graesser's model for the strain-rate-dependent hysteresis behavior of superelastic SMA wires. Thamburaja [10] developed thermomechanically coupled and nonlocal phenomenological theory for SMAs to investigate the nonisothermal behavior during tensile superelastic deformation. The author numerically showed the trend of stress-strain responses by increasing the strain rate: a wider hysteresis loop and a significantly larger hardening and softening during the forward loading process and the reverse loading process, respectively. Morin et al. [11] developed a model for SMAs that takes into account thermomechanical coupling by considering two main heat sources: intrinsic

dissipation and latent heat. However, for high strain rates, only qualitative agreement is achieved for thermal results.

In this research, the effect of the strain rate on the pseudoelastic behavior of SMA wires is experimentally and numerically investigated. Experimental tests of the thermomechanical coupling in SMA are analyzed to evaluate the parameters for a numerical SMA model with strain-rate dependency. As a strain rate increases, the forward and reverse transformation critical stress commence at a higher stress value. The slope of the transformation plateau also increases. Thus, a new form of transformation parameter is proposed to improve agreement with experimental data. The SMAs' rate-dependent behavior is modeled by coupling of the rate-independent kinetic rules with the heat equation. With an improved thermomechanical constitutive model, the author can fairly accurately predict the strain-rate-dependent behavior of pseudoelastic SMA wires at various loading rates.

2. Thermodynamics for the Constitutive Law

It is assumed that the thermodynamics of SMAs are fully described by the set of variables $(\boldsymbol{\varepsilon}, T, \xi)$, where $\boldsymbol{\varepsilon}$ is the Green strain and ξ is an internal variable representing the stage of the transformation. ξ is defined as the martensite fraction of the material, which varies from zero to one with unity representing 100% martensite, and its value is governed by temperature and stress. The strain of an SMP material can be decomposed into two parts: $\boldsymbol{\varepsilon} = \boldsymbol{\varepsilon}_{\text{el}} + \boldsymbol{\varepsilon}_{\text{in}}$, where $\boldsymbol{\varepsilon}_{\text{el}}$ is the thermoelastic strain and ε_{in} is the inelastic strain due to phase transformation. The Helmholtz free energy per unit mass which depends on state variables and internal variables is chosen as

$$\Phi = \Phi\left(\boldsymbol{\varepsilon}, T, \boldsymbol{\varepsilon}_{\text{el}}, \boldsymbol{\varepsilon}_{\text{in}}, \xi\right) = \Phi\left(\boldsymbol{\varepsilon}_{\text{el}}, T, \xi\right). \tag{1}$$

The Clausius-Duhem inequality with

$$\dot{\Phi} = \frac{\partial \Phi}{\partial \boldsymbol{\varepsilon}_{\text{el}}} : \dot{\boldsymbol{\varepsilon}}_{\text{el}} + \frac{\partial \Phi}{\partial T}\dot{T} + \frac{\partial \Phi}{\partial \xi}\dot{\xi} \tag{2}$$

can be obtained based on the first and second law of thermodynamics:

$$\left(\boldsymbol{\sigma} - \rho\frac{\partial \Phi}{\partial \boldsymbol{\varepsilon}_{\text{el}}}\right) : \dot{\boldsymbol{\varepsilon}}_{\text{el}} - \rho\left(s + \frac{\partial \Phi}{\partial T}\right)\dot{T} - \rho\frac{\partial \Phi}{\partial \xi}\dot{\xi} - \frac{\vec{q}}{T} \cdot \overrightarrow{\text{grad}}\, T \geq 0, \tag{3}$$

where $\boldsymbol{\sigma}$, s, T, and $\vec{q}$ represent the stress tensor, the specific entropy per unit mass, the temperature, and the heat flux vector, respectively.

A sufficient condition for (3) to hold for every choice of $\dot{\boldsymbol{\varepsilon}}_{\text{el}}$ and $\dot{T}$ is that their respective coefficients must vanish, thus yielding

$$\boldsymbol{\sigma} = \rho\frac{\partial \Phi}{\partial \boldsymbol{\varepsilon}_{\text{el}}}, \tag{4}$$

$$s = -\frac{\partial \Phi}{\partial T}. \tag{5}$$

In an analogous manner, the thermodynamic forces associated with the internal variables can be defined by

$$\Lambda = \rho\frac{\partial \Phi}{\partial \xi}. \tag{6}$$

Heat transfer between SMAs and the surrounding environment is considered. The heat transfer caused by heat flux can be described using the following equation:

$$\vec{q} = k \cdot \overrightarrow{\text{grad}}\, T, \tag{7}$$

where k is the thermal conductivity.

From the energy conservation equation, $\rho\dot{e}$ can be replaced by the expression derived from the specific internal energy, $e = \Phi + Ts$:

$$\rho\dot{e} = \rho\dot{\Phi} + \rho T\dot{s} + \rho\dot{T}s \tag{8}$$

and $\dot{\Phi}$ can be expressed as a function of the state variables $(\boldsymbol{\varepsilon}_{\text{el}}, T, \xi)$ using (4), (5), and (6), so that

$$\dot{\Phi} = \frac{1}{\rho}\boldsymbol{\sigma} : \dot{\boldsymbol{\varepsilon}}_{\text{el}} - s\dot{T} + \frac{1}{\rho}\Lambda\dot{\xi}. \tag{9}$$

By substituting (9) into (8), $\rho\dot{e}$ can be derived:

$$\rho\dot{e} = \boldsymbol{\sigma} : \dot{\boldsymbol{\varepsilon}}_{\text{el}} + \Lambda\dot{\xi} + \rho T\dot{s}. \tag{10}$$

The first principle of thermodynamics, $\rho\dot{e} - \boldsymbol{\sigma} : \dot{\boldsymbol{\varepsilon}} + r - \text{div}\,\vec{q} = 0$, can be rewritten using (10) as

$$\boldsymbol{\sigma} : \dot{\boldsymbol{\varepsilon}}_{\text{el}} + \Lambda\dot{\xi} + \rho T\dot{s} = \boldsymbol{\sigma} : \dot{\boldsymbol{\varepsilon}} + r - \text{div}\,\vec{q}. \tag{11}$$

Entropy is a function of the state variables, so the entropy rate can be expressed with (5) and (6) as

$$\begin{aligned} \dot{s} &= -\frac{\partial^2 \Phi}{\partial \boldsymbol{\varepsilon}_{\text{el}} \partial T} : \dot{\boldsymbol{\varepsilon}}_{\text{el}} - \frac{\partial^2 \Phi}{\partial T^2}\dot{T} - \frac{\partial^2 \Phi}{\partial \xi \partial T}\dot{\xi} \\ &= -\frac{1}{\rho}\frac{\partial \boldsymbol{\sigma}}{\partial T} : \dot{\boldsymbol{\varepsilon}}_{\text{el}} + \frac{\partial s}{\partial T}\dot{T} - \frac{1}{\rho}\frac{\partial \Lambda}{\partial T}\dot{\xi}. \end{aligned} \tag{12}$$

By introducing the specific heat defined by $C_p = T(\partial s/\partial T)$, and taking into account Fourier's law, $\text{div}\,\vec{q} = -k \cdot \text{div}(\overrightarrow{\text{grad}}\, T) = -k\nabla^2 T$, (11) can be modified using $\dot{\boldsymbol{\varepsilon}}_{\text{in}} = \dot{\boldsymbol{\varepsilon}} - \dot{\boldsymbol{\varepsilon}}_{\text{el}}$:

$$k\nabla^2 T = \rho C_p\dot{T} - \boldsymbol{\sigma} : \dot{\boldsymbol{\varepsilon}}_{\text{in}} + \Lambda\dot{\xi} - r - T\left(\frac{\partial \boldsymbol{\sigma}}{\partial T} : \dot{\boldsymbol{\varepsilon}}_{\text{el}} + \frac{\partial \Lambda}{\partial T}\dot{\xi}\right). \tag{13}$$

Under the assumptions that there is no internal heat production generated by external sources, that is, $r = 0$, there is no thermomechanical coupling; that is, $(\partial\sigma/\partial T) : \dot{\boldsymbol{\varepsilon}}_{\text{el}} = 0$ and $(\partial\Lambda/\partial T)\dot{\xi} = 0$. A uniform temperature in the SMA is assumed under loading. The heat flux is caused by heat transfer between the SMA and the surrounding environment due to the temperature difference. The heat transfer equation can be described using $\dot{Q} = h \cdot (T - T_o)$, where $\dot{Q}$ is the transient rate of heat flow, T and T_o are the transient temperature

of the SMA under loading and environment temperature, respectively, and h is the heat transfer coefficient, which should include not only the heat convection but also the heat contact between the SMA wire specimen and the gripping fixture at the end of the specimen. Here, the heat transfer coefficient has a dimension of $W^{\circ}C^{-1}$. It is assumed that the temperature of the gripping fixture and the environment should be a constant, T_o. The divergence of heat flux (div $\vec{q}$) can be estimated from heat transfer per unit volume (V): $\text{div}\,\vec{q} = -k\nabla^2 T = h/V \cdot (T - T_o)$; (13) can be rewritten as

$$\rho C_p \dot{T} = \boldsymbol{\sigma} : \dot{\boldsymbol{\varepsilon}}_{\text{in}} - \Lambda\dot{\xi} + \frac{h}{V} \cdot (T - T_o). \tag{14}$$

Thus, for materials like superelastic SMAs, only part of the mechanical input energy is stored in the form of elastic strain energy; the remaining part of the mechanical input energy is dissipated due to the inelastic deformation. Such energy dissipation usually contributes to the temperature variation in the SMA specimen under loading and thus affects the material behavior of SMAs. The term $\boldsymbol{\sigma} : \dot{\boldsymbol{\varepsilon}}_{\text{in}}$ in (14) represents the time rate of mechanical energy dissipation due to the inelastic deformation; the term $\Lambda\dot{\xi}$ represents the rate of latent heat, and the negative sign means the austenite to martensite transformation is exothermic, while the martensite to austenite transformation is endothermic. Thus (14) means that at any instant the heat generation due to the inelastic dissipation is equal to the specific heat absorbed by the specimen plus the heat loss to the environment.

3. Constitutive SMA Equations with Strain-Rate Dependence

The rate form of 1D constitutive equations of SMA wire can be obtained by modifying the thermodynamic equations. The model consists of three equations: the constitutive equation, the transformation equation, and the energy balance equation. The constitutive equation can be expressed as a description of the increment of strain, $\dot{\varepsilon}$, in terms of the increments of stress, $\dot{\sigma}$, temperature, $\dot{T}$, and the martensite fraction, $\dot{\xi}$, by differentiating (4):

$$\dot{\sigma} = D\dot{\varepsilon} + \theta\dot{T} + \Omega\dot{\xi}, \tag{15}$$

where D is Young's modulus, θ is related to the thermal expansion coefficient, and Ω is representative of the transformation tensor for the SMAs as defined by the following equations:

$$\begin{aligned} D &\equiv \rho\frac{\partial^2\Phi}{\partial\varepsilon_{\text{el}}\partial\varepsilon}, \\ \theta &\equiv \rho\frac{\partial^2\Phi}{\partial\varepsilon_{\text{el}}\partial T}, \\ \Omega &\equiv \rho\frac{\partial^2\Phi}{\partial\varepsilon_{\text{el}}\partial\xi}. \end{aligned} \tag{16}$$

The inelastic and elastic strain can be expressed as

$$\begin{aligned} \varepsilon &= \varepsilon_{\text{el}} + \varepsilon_{\text{in}}, \\ \varepsilon_{\text{in}} &= \varepsilon_l\xi, \\ \varepsilon_{\text{el}} &= \varepsilon - \varepsilon_l\xi, \end{aligned} \tag{17}$$

where ε_l is the maximum residual strain. The Helmholtz free energy for superelastic SMA, $\Phi(\varepsilon_{\text{el}}, T, \xi)$, is assumed to be of the following form:

$$\begin{aligned} \Phi = {} & \frac{D}{2\rho}\varepsilon_{\text{el}}^2 + \frac{L}{T_{\text{cr}}}(T - T_{\text{cr}})\,\xi \\ & -C_p T\ln\left(\frac{T}{T_o}\right) + \frac{D}{\rho}\varepsilon_{\text{el}}\alpha(T - T_o). \end{aligned} \tag{18}$$

The transformation equation, which relates the increment of the martensite fraction to the transformation strain, has been well established by Tanaka [12], Liang and Rogers [13], and Brinson [14]. The transformation kinetics represent the martensite fraction as a function of stress and temperature. In order to further improve the simulated behavior of superelastic SMAs, Brinson's model of transformation kinetics is used for a rate-dependent constitutive model. In this model, a separation of this variable into two parts is proposed based on the micromechanics of SMA materials. ξ can be defined by

$$\xi = \xi_T + \xi_S, \tag{19}$$

where ξ_T represents the fraction of the material that is purely temperature-induced martensite with multiple variants and ξ_S denotes the fraction of the material that has been transformed by stress into a single martensitic variant. Young's modulus, D, and the material property, Ω, can be defined as a function of ξ:

$$\begin{aligned} D &= E^A + \xi\left(E^M - E^A\right), \\ \Omega &= -\varepsilon_l D, \end{aligned} \tag{20}$$

where E^A and E^M are the modulus values of the SMA as austenite and martensite, respectively.

The evolution of the martensite fraction during the phase transformation in Brinson's model is defined by the following equations.

Transformation from austenite to martensite:
for $T > M_s$ and $\sigma_s^{\text{cr}} + C_M(T - M_s) < \sigma < \sigma_f^{\text{cr}} + C_M(T - M_s)$,

$$\begin{aligned} \xi_S = {} & \frac{1 - \xi_{so}}{2}\cos\left\{\frac{\pi}{\sigma_s^{\text{cr}} - \sigma_f^{\text{cr}}} \times \left[\sigma - \sigma_f^{\text{cr}} - C_M(T - M_S)\right]\right\} \\ & + \frac{1 + \xi_{so}}{2}, \end{aligned} \tag{21a}$$

$$\xi_T = \xi_{To} - \frac{\xi_{To}}{1 - \xi_{So}}(\xi_S - \xi_{So}). \tag{21b}$$

Transformation from martensite to austenite:
for $T > A_s$ and $C_A(T - A_f) < \sigma < C_A(T - A_s)$,

$$\xi = \frac{\xi_o}{2}\left\{\cos\left[a_A\left(T - A_s - \frac{\sigma}{C_A}\right)\right] + 1\right\}, \tag{22a}$$

$$\xi_S = \xi_{so} - \frac{\xi_{so}}{\xi_o}\left(\xi_o - \xi\right), \tag{22b}$$

$$\xi_T = \xi_{To} - \frac{\xi_{To}}{\xi_o}\left(\xi_o - \xi\right), \tag{22c}$$

where C_M and C_A are parameters and σ_s^{cr} and σ_f^{cr} are the critical stresses at the start and finish of the conversion of martensitic variants. a_A is defined by $a_A = \pi/(A_f - A_s)$.

The transformation equations for forward (austenite to martensite) and reverse (martensite to austenite) directions can be obtained by differentiating (21a), (21b), (22a), (22b), and (22c), respectively:

$$\dot{\xi} = -\frac{1-\xi_o}{2}\sin\left\{\frac{\pi}{\sigma_s^{\mathrm{cr}} - \sigma_f^{\mathrm{cr}}}\left[\sigma - \sigma_f^{\mathrm{cr}} - C_M\left(T - M_s\right)\right]\right\} \times\left(\frac{\pi}{\sigma_s^{\mathrm{cr}} - \sigma_f^{\mathrm{cr}}}\dot{\sigma} - \frac{\pi C_M}{\sigma_s^{\mathrm{cr}} - \sigma_f^{\mathrm{cr}}}\dot{T}\right), \tag{23a}$$

$$\dot{\xi} = -\frac{\xi_o}{2}\sin\left[a_A\left(T - A_s - \frac{\sigma}{C_A}\right)\right]\cdot\left(a_A\dot{T} - \frac{a_A}{C_A}\dot{\sigma}\right). \tag{23b}$$

From the energy balance equation derived in (14), the rate form of temperature variation can be obtained by substituting (17) and (18) as

$$\dot{T} = \frac{1}{\rho C_p}\left[\sigma\varepsilon_l - \frac{E^M - E^A}{2}\left(\varepsilon - \varepsilon_l\xi\right)^2 + D\varepsilon_l\left(\varepsilon - \varepsilon_l\xi\right) + \frac{\rho L}{T_{\mathrm{cr}}}\left(T - T_{\mathrm{cr}}\right) + \left(E^M - E^A\right)\varepsilon_{\mathrm{el}}\alpha\left(T - T_o\right) - D\varepsilon_l\alpha\left(T - T_o\right)\right]\dot{\xi} - \frac{h}{\rho C_p V}\left(T - T_o\right). \tag{24}$$

The rate forms of the constitutive models of (15), (23a), (23b), and (24) are used for the numerical analysis. In order to solve for the three variants σ, T, and ξ, these three constitutive equations need to be integrated simultaneously. By solving algebraic equations involving the first power of $\dot{\sigma}$, $\dot{T}$, or $\dot{\xi}$, the constitutive equations can be rewritten into the following forms.

Austenite to martensite:

$$\dot{\sigma} = \frac{C_1 - C_1C_4C_7}{1 - C_2C_6 - C_3C_4C_6 - C_4C_7}\dot{\varepsilon} + \frac{C_3C_5 + C_2C_5C_7}{1 - C_2C_6 - C_3C_4C_6 - C_4C_7}, \tag{25a}$$

$$\dot{T} = \frac{C_1C_4C_6}{1 - C_2C_6 - C_3C_4C_6 - C_4C_7}\dot{\varepsilon} + \frac{C_5 - C_2C_5C_6}{1 - C_2C_6 - C_3C_4C_6 - C_4C_7}, \tag{25b}$$

$$\dot{\xi} = \frac{C_1C_6}{1 - C_2C_6 - C_3C_4C_6 - C_4C_7}\dot{\varepsilon} + \frac{C_3C_5C_6 - C_5C_7}{1 - C_2C_6 - C_3C_4C_6 - C_4C_7}. \tag{25c}$$

Martensite to austenite:

$$\dot{\sigma} = \frac{C_1 - C_1C_4C_9}{1 - C_2C_8 - C_3C_4C_8 - C_4C_9}\dot{\varepsilon} + \frac{C_3C_5 + C_2C_5C_9}{1 - C_2C_8 - C_3C_4C_8 - C_4C_9}, \tag{26a}$$

$$\dot{T} = \frac{C_1C_4C_8}{1 - C_2C_8 - C_3C_4C_8 - C_4C_9}\dot{\varepsilon} + \frac{C_5 - C_2C_5C_8}{1 - C_2C_8 - C_3C_4C_8 - C_4C_9}, \tag{26b}$$

$$\dot{\xi} = \frac{C_1C_8}{1 - C_2C_8 - C_3C_4C_8 - C_4C_9}\dot{\varepsilon} + \frac{C_3C_5C_8 - C_5C_9}{1 - C_2C_8 - C_3C_4C_8 - C_4C_9}. \tag{26c}$$

Each parameter can be defined as follows:

$$C_1 \equiv D\left(\xi\right), \quad C_2 \equiv \Omega\left(\xi\right), \quad C_3 \equiv \theta, \tag{27a}$$

$$C_4 \equiv \frac{1}{\rho C_p}\left[\sigma\varepsilon_L + \frac{E^A - E^M}{2}\left(\varepsilon - \varepsilon_L\xi\right)^2 + \rho L\right], \quad C_5 \equiv -\frac{h}{\rho C_p V}\left(T - T_o\right), \tag{27b}$$

$$C_6 \equiv -\frac{1-\xi_o}{2}\sin\left\{\frac{\pi}{\sigma_s^{\mathrm{cr}} - \sigma_f^{\mathrm{cr}}}\left[\sigma - \sigma_f^{\mathrm{cr}} - C_M\left(T - M_s\right)\right]\right\} \times\frac{\pi}{\sigma_s^{\mathrm{cr}} - \sigma_f^{\mathrm{cr}}}, \tag{27c}$$

$$C_7 \equiv \frac{1-\xi_o}{2}\sin\left\{\frac{\pi}{\sigma_s^{\mathrm{cr}}-\sigma_f^{\mathrm{cr}}}\left[\sigma-\sigma_f^{\mathrm{cr}}-C_M\left(T-M_s\right)\right]\right\} \times \frac{\pi C_M}{\sigma_s^{\mathrm{cr}}-\sigma_f^{\mathrm{cr}}}, \tag{27d}$$

$$C_8 \equiv \frac{\xi_o}{2}\sin\left[a_A\left(T-A_s-\frac{\sigma}{C_A}\right)\right]\cdot\frac{a_A}{C_A}, \qquad C_9 \equiv -\frac{\xi_o}{2}\sin\left[a_A\left(T-A_s-\frac{\sigma}{C_A}\right)\right]\cdot a_A. \tag{27e}$$

These differential equations are simultaneously solved using the fourth-order Runge-Kutta method.

4. Experimental Characterization of an SMA Wire

To characterize the thermomechanical behaviors of an SMA wire, the author takes experimental measurements of an SMA wire (Alloy S), which is manufactured by the MEMRY Corporation. Alloy S, a diameter 2.31 mm, shows pseudoelastic behavior at room temperature. For the loading and unloading test at various temperatures, MTS 810 universal testing machine with thermal chamber is used. To measure the strain, an extensometer (MTS 634) with a 25 mm gauge length is used. The thermocouple (K type) is adhered on middle of the specimen to observe the temperature variation of the SMA with strain rates. To characterize the temperature-induced transformation, differential scanning calorimeter (DSC) was utilized with a constant rate of heating and cooling, 10°C /min.

The training was performed by applying 15 sequential loading/unloading cycles to stabilize the alloy. With the material being satisfactorily stabilized, the characterization process experiment was carried out to derive final material parameters. Continuing, isothermal loading is applied to the trained wire specimens at different constant temperatures (25, 30, 40, and 50°C). By noting where transformations begin and end, a detailed phase diagram can be constructed. Figure 1 shows the pseudoelastic curve for a constant temperature of 25°C, which illustrates detailed material parameters. Here, E^A and E^M are measured in a straightforward manner. The critical stresses for initiation and completion of phase transformation are determined. These stresses are denoted as σ^{M_s} and σ^{M_f} for martensite and σ^{A_s} and σ^{A_f} for austenite. The values for theses stresses at a test temperature of 25°C are shown in Figure 1. In addition to the determination of the final phase diagram, the maximum transformation strain, ε_l, was also derived. The maximum transformation strain is equivalent to the amount of strain indicated when the martensitic elastic stress response is extrapolated to the zero-stress axis. By examining the five isothermal pseudoelastic tests performed, one can determine the stresses for the initiation and completion of both transformations at five distinct temperatures. Construction of the phase diagram which proceeded using this experimental data is shown in Figure 2. The critical stresses, σ_{cr}^s and σ_{cr}^f, represent the start and finish stresses for the detwinning of martensite and are assumed to be constant to fully describe the configuration of the phase diagram. The parameters for the constitutive model used in this study to simulate the pseudoelastic behavior of SMA wire are experimentally measured and given in Table 1. It is seen in Figure 3 that the model with the presented thermomechanical parameters can predict the pseudoelastic behavior of SMA wire quite well.

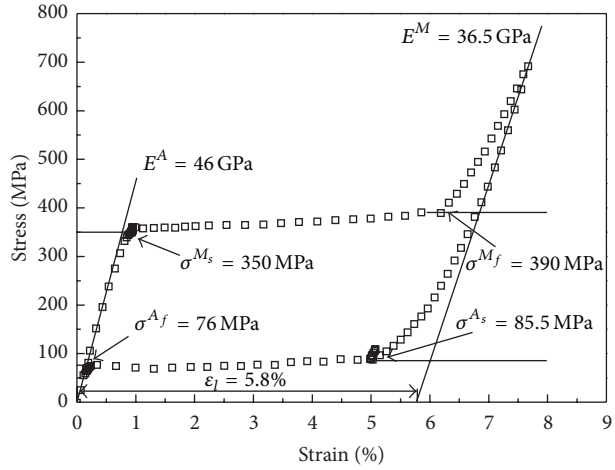

Figure 1: Pseudoelastic behavior of the SMA for temperature of 25°C.

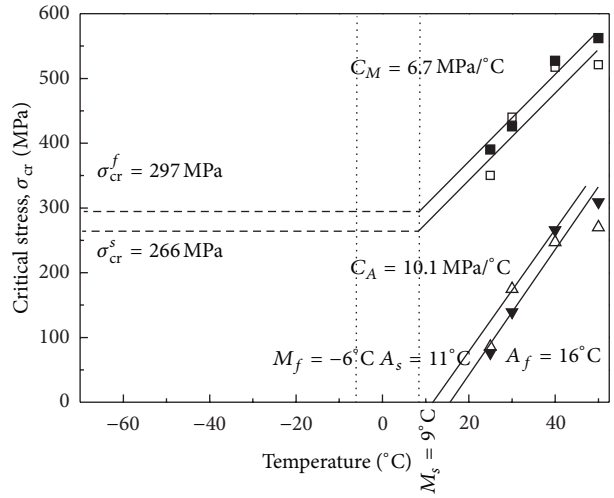

Figure 2: Temperature dependence of critical stress for inducing phase transformation.

5. The Strain-Rate Effect on the Pseudoelastic Behaviors of an SMA Wire

The pseudoelastic behaviors of SMA wires for a variety of loading rates are measured experimentally in Figure 4. Two major thermomechanical behaviors of the pseudoelastic SMA wires under varying loading rates can be captured: the increasing of the critical stresses of phase transformation

Table 1: Material properties of SMA wire.

Moduli and thermal expansion	$E^A = 46$ GPa $E^M = 36.5$ GPa $\alpha = 0.0$ MPa/°C
Transformation temperatures	$M_f = -6$°C $M_s = 9$°C $A_s = 11$°C $A_f = 16$°C
Transformation constants	$C_M = 6.7$ MPa/°C $C_A = 10.1$ MPa/°C $\sigma_{cr}^s = 266$ MPa $\sigma_{cr}^f = 297$ MPa
Maximum residual strain	$\varepsilon_l = 0.058$
Density	$\rho = 6465\ \mathrm{kgm}^{-3}$
Thermodynamic constants	$C_p = 2667\ \mathrm{Jkg}^{-1}\mathrm{°C}^{-1}$ $L = 24200\ \mathrm{Jkg}^{-1}$ $h = 0.042\ \mathrm{W°C}^{-1}$

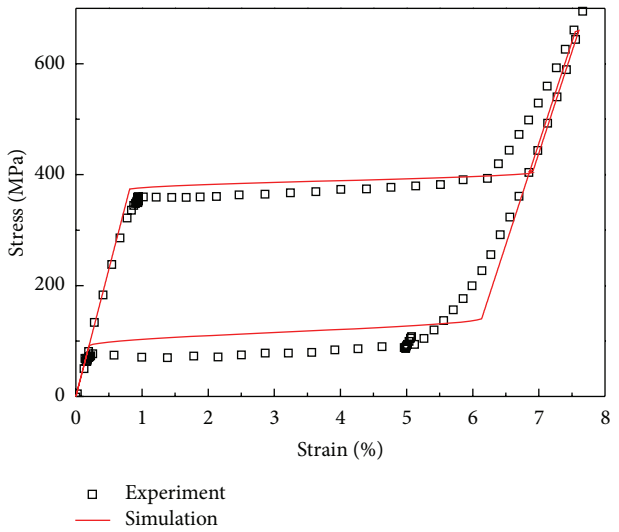

Figure 3: Comparison of pseudoelastic behavior at temperature of 25°C.

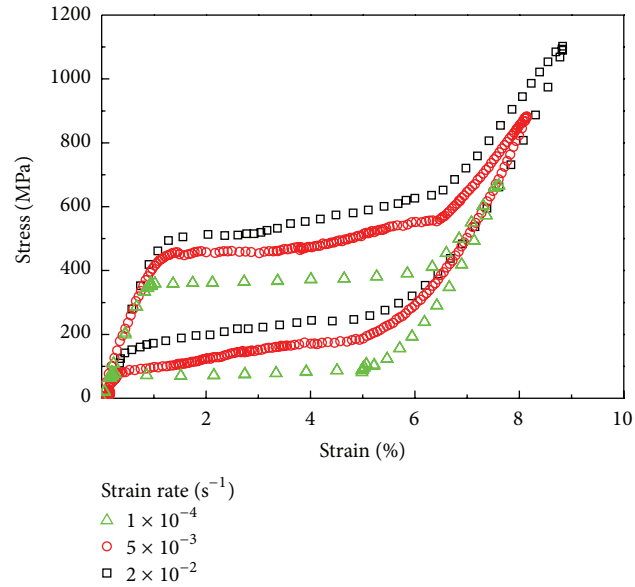

Figure 4: Strain-rate effect on pseudoelastic behavior.

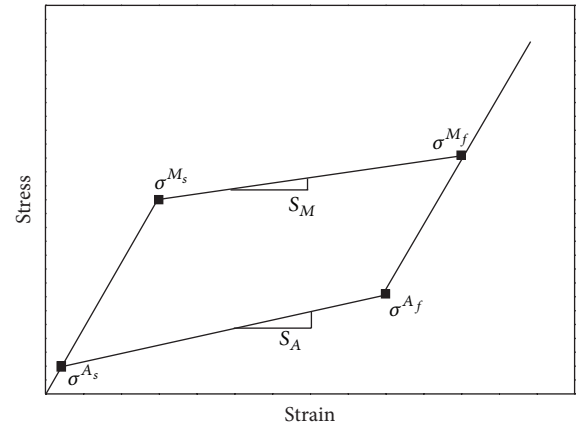

Figure 5: Schematic representation of the critical stresses and the slope of transformation plateau.

such as σ^{M_s}, σ^{M_f}, σ^{A_s}, and σ^{A_f} and the increased slope of the transformation plateau with increasing loading rates. Similar experimental results were also reported in [2]. So, it is necessary to take account of this point to the numerical model of SMAs. Even if the transformation stresses as well as the slope of each transformation line are affected by strain rates, the stress-temperature phase diagram of Brinson's model cannot consider these effects.

In this research, the material parameters C_M and C_A, which represent the slope of critical stresses variation with respect to temperature, are newly proposed as depending on strain rates:

$$C_M^* = C_M + S_M \cdot \sin(0.05 \cdot \dot{\varepsilon}), \tag{28a}$$

$$C_A^* = C_A + S_A \cdot \sin(0.05 \cdot \dot{\varepsilon}), \tag{28b}$$

where S_M and S_A indicate a variation of the inclination from σ^{M_s} to σ^{M_f} and from σ^{A_s} to σ^{A_f} with respect to loading rates, respectively (Figure 5). The parameters are phenomenologically developed by fitting the variation curves of critical stresses with respect to strain rates based on the experiments and can be simply handled and implemented into the SMA constitutive equations. The values of S_M and S_A are experimentally measured as follows:

$$S_M = 15665.4\ \mathrm{MPa/°C},$$
$$S_A = 8195.6\ \mathrm{MPa/°C}. \tag{29}$$

Figures 6, 7, and 8 show the comparisons of pseudoelastic behaviors of SMA wires with respect to strain rates. The simulation results are compared with the result without rate dependency to show the effectiveness of the developed model for the consideration of the strain-rate effect on

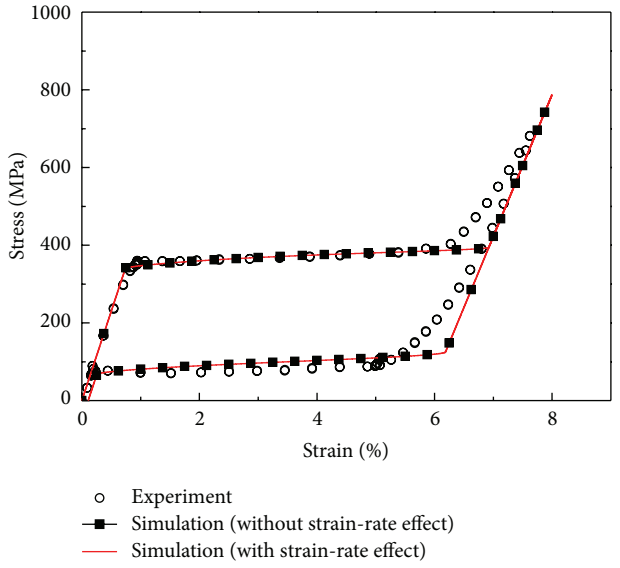

Figure 6: Comparisons of pseudoelastic behavior at strain rate of $1 \times 10^{-4}\ s^{-1}$.

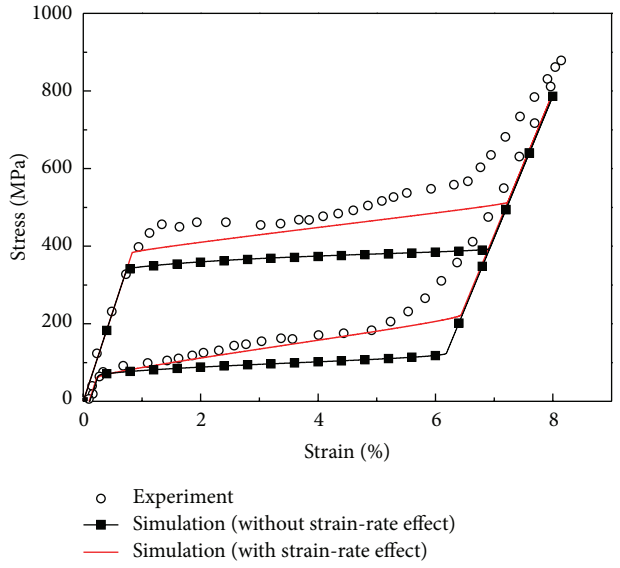

Figure 7: Comparisons of pseudoelastic behavior at strain rate of $5 \times 10^{-3}\ s^{-1}$.

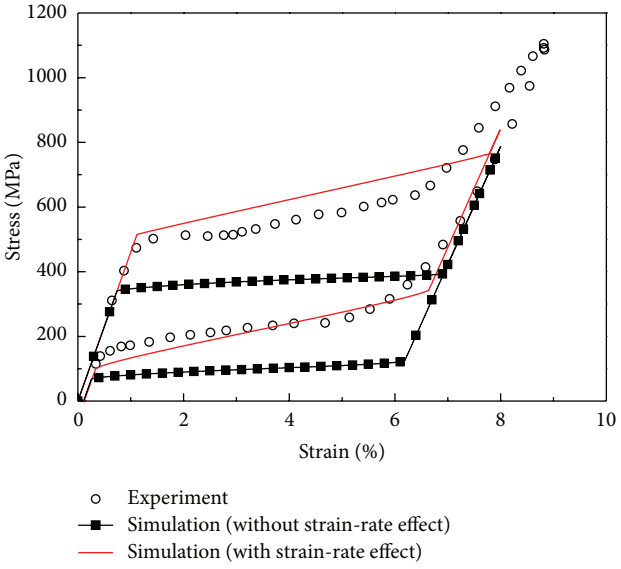

Figure 8: Comparisons of pseudoelastic behavior at strain rate of $2 \times 10^{-2}\ s^{-1}$.

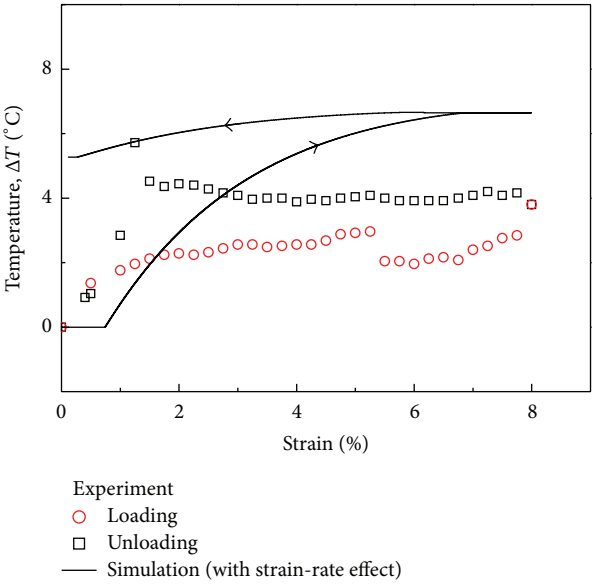

Figure 9: Temperature variation at strain rate of $1 \times 10^{-4}\ s^{-1}$.

the pseudoelastic behaviors of SMAs. In the case of strain rate of $1 \times 10^{-4}s^{-1}$, there is a good agreement between the simulation and the experiment. However, the higher the strain rates, the bigger the discrepancy between the simulation without strain-rate effect and the experiment results. For the strain rates of $5 \times 10^{-3}s^{-1}$ and $2 \times 10^{-2}s^{-1}$, the present model can sufficiently follow the variation of phase transformation stresses (σ^{M_s}, σ^{M_f}, σ^{A_s}, and σ^{A_f}) as well as the increased slope of the transformation plateau. Thus, the present model can effectively predict the pseudoelastic behaviors of SMAs with respect to strain rates. Figures 9, 10, and 11 present the experimental and simulation results of temperature variation in SMA specimens. It is seen that the proposed constitutive model is able to properly predict the trend of temperature change in pseudoelastic SMAs. In a strain rate with a quasistatic loading of $1 \times 10^{-4}s^{-1}$, there is a negligible temperature change. However, the temperature variation is slightly increased as the strain rates are further increased. Although the simulated temperature agrees fairly well with the experiment for the strain rates, the presented model seems to underpredict the temperature change. Such a discrepancy may arise from either inaccuracies with respect to the identified model parameters or errors in temperature measurement. Figure 12 shows the hysteresis of martensite fraction at various strain rates. In loading process, the

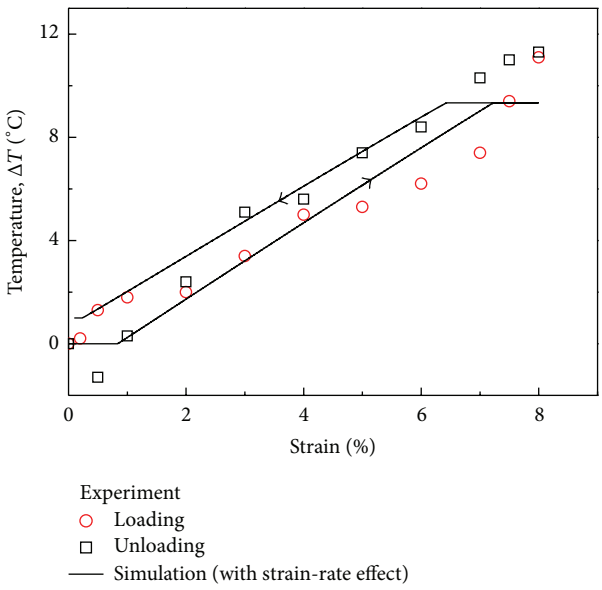

Figure 10: Temperature variation at strain rate of 5×10^{-3} s^{-1}.

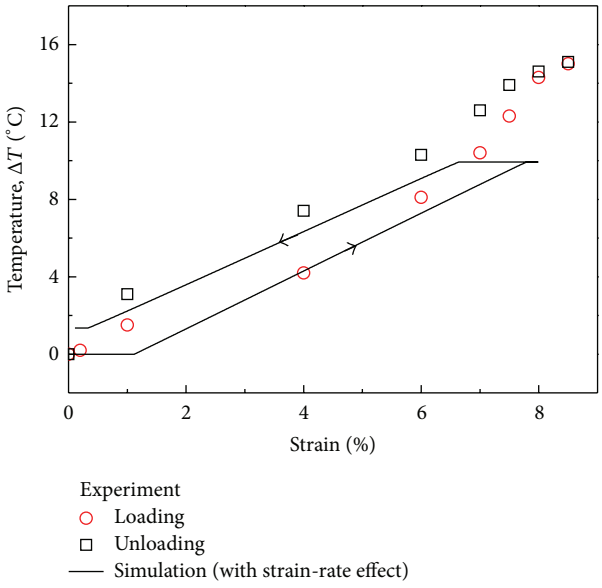

Figure 11: Temperature variation at strain rate of 2×10^{-2} s^{-1}.

forward phase transformation (austenite to martensite) is retarded by increasing strain rates, but the reverse phase transformation (martensite to austenite) begins earlier in unloading process. Moreover, the slope of martensite fraction with respect to strain decreases by increasing strain rates.

6. Conclusion

In our experimental and numerical investigation of the thermomechanical behaviors of SMAs, the author finds the following: the strain rate affects the phase transformation stresses as well as the slope of the transformation plateau

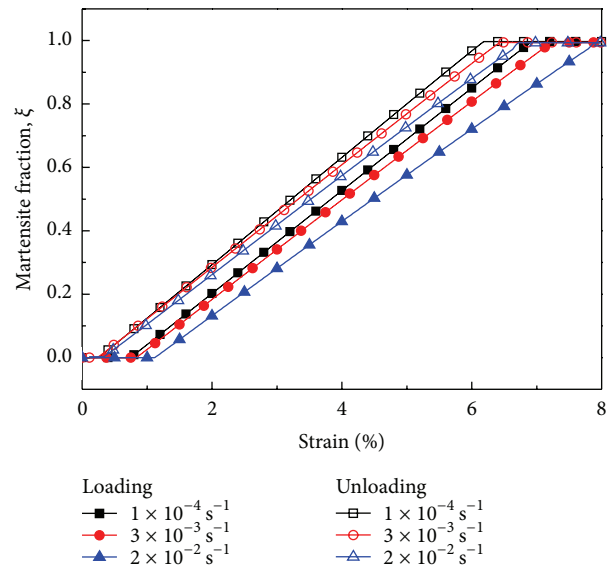

Figure 12: Hysteresis of martensite fraction at various strain rates.

and the temperature variation is slightly increased at further increased strain rates. The author also proposes a 1D incremental formulation of the SMA model with strain-rate dependence. This numerical model is able to provide good predictions of the thermomechanical characteristics of SMAs such as the pseudoelastic strain-stress curves and the temperature variation with respect to strain rates. The advantages of the presented model are the simplicity, the possibility of implementing a robust solution algorithm, and the ability to predict fairly well experimental results obtained at different strain rates. It is expected that the model should be useful for designing and evaluating damping devices using the pseudoelastic characteristics of SMAs.

Conflict of Interests

The author declares that there is no conflict of interests regarding the publication of this paper.

Acknowledgment

This research was supported by Space Core Technology Development Program funded by the Ministry of Education, Science and Technology (NRF-2012M1A3A3A02033484).

References

[1] K. Mukherjee, S. Sircar, and N. B. Dahotre, "Thermal effects associated with stress-induced martensitic transformation in a Ti-Ni alloy," *Materials Science and Engineering*, vol. 74, no. 1, pp. 75–84, 1985.

[2] H. Tobushi, Y. Shimeno, T. Hachisuka, and K. Tanaka, "Influence of strain rate on superelastic properties of TiNi shape memory alloy," *Mechanics of Materials*, vol. 30, no. 2, pp. 141–150, 1998.

[3] S. Nemat-Nasser and W. Guo, "Superelastic and cyclic response of NiTi SMA at various strain rates and temperatures," *Mechanics of Materials*, vol. 38, no. 5-6, pp. 463–474, 2006.

[4] H. Soul, A. Isalgue, A. Yawny, V. Torra, and F. C. Lovey, "Pseudoelastic fatigue of NiTi wires: frequency and size effects on damping capacity," *Smart Materials and Structures*, vol. 19, no. 8, Article ID 085006, 7 pages, 2010.

[5] S. Sun and R. K. N. D. Rajapakse, "Simulation of pseudoelastic behaviour of SMA under cyclic loading," *Computational Materials Science*, vol. 28, no. 3-4, pp. 663–674, 2003.

[6] S. Zhu and Y. Zhang, "A thermomechanical constitutive model for superelastic SMA wire with strain-rate dependence," *Smart Materials and Structures*, vol. 16, no. 5, pp. 1696–1707, 2007.

[7] M. Kadkhodaei, R. K. N. D. Rajapakse, M. Mahzoon, and M. Salimi, "Modeling of the cyclic thermomechanical response of SMA wires at different strain rates," *Smart Materials and Structures*, vol. 16, no. 6, pp. 2091–2101, 2007.

[8] F. Auricchio, D. Fugazza, and R. DesRoches, "Rate-dependent thermo-mechanical modelling of superelastic shape-memory alloys for seismic applications," *Journal of Intelligent Material Systems and Structures*, vol. 19, no. 1, pp. 47–61, 2008.

[9] W. Ren, H. Li, and G. Song, "A one-dimensional strain-rate-dependent constitutive model for superelastic shape memory alloys," *Smart Materials and Structures*, vol. 16, pp. 191–197, 2007.

[10] P. Thamburaja, "A finite-deformation-based phenomenological theory for shape-memory alloys," *International Journal of Plasticity*, vol. 26, no. 8, pp. 1195–1219, 2010.

[11] C. Morin, Z. Moumni, and W. Zaki, "A constitutive model for shape memory alloys accounting for thermomechanical coupling," *International Journal of Plasticity*, vol. 27, no. 5, pp. 748–769, 2011.

[12] K. Tanaka, "A thermomechanical sketch of shape memory effect: one-dimensional tensile behavior," *Res Mechanica*, vol. 2, no. 3, pp. 59–72, 1986.

[13] C. Liang and C. A. Rogers, "One-dimensional thermomechanical constitutive relations for shape memory materials," *Journal of Intelligent Material Systems and Structures*, vol. 1, pp. 207–234, 1990.

[14] L. C. Brinson, "One-dimensional constitutive behavior of shape memory alloys: thermomechanical derivation with non-constant material functions and redefined martensite internal variable," *Journal of Intelligent Material Systems and Structures*, vol. 4, no. 2, pp. 229–242, 1993.